

A new soil freeze/thaw discriminant algorithm using AMSR-E passive microwave imagery

Tianjie Zhao,^{1,2} Lixin Zhang,^{1,2*} Lingmei Jiang,^{1,2} Shaojie Zhao,^{1,2} Linna Chai^{1,2} and Rui Jin³

¹ State Key Laboratory of Remote Sensing Science, Jointly Sponsored by Beijing Normal University and Institute of Remote Sensing Applications, CAS, Beijing 100875, China

² School of Geography and Remote Sensing Science, Beijing Normal University, Beijing 100875, China

³ Cold and Arid Regions Environmental and Engineering Research Institute, CAS, Lanzhou, Gansu 730000, China

Abstract:

The soil freeze–thaw controls the hydrological and carbon cycling and thus affects water and energy exchanges at land surface. This article reported a newly developed algorithm for distinguishing the freeze/thaw status of surface soil. The algorithm was based on information from Advanced Microwave Scanning Radiometer Enhanced (AMSR-E) which records brightness temperature (Tb) in the afternoon and after midnight. The criteria and discriminant functions were obtained from both radiometer observations and model simulations. First of all, the microwave radiation from freeze–thaw soil was examined by carrying out experimental measurements at 18.7 and 36.5 GHz using a Truck-mounted Multi-frequency Microwave Radiometer (TMMR) in the Heihe River of China. The experimental results showed that the soil moisture is a key component that differentiates the microwave radiation behaviours during the freeze–thaw process, and the differences in soil temperature and emissivity between frozen and thawed soils were found to be the most important criteria. Secondly, a combined model was developed to consider the impacts of complex ground surface conditions on the discrimination. The model simulations quite followed the trend of *in situ* observations with an overall relation coefficient (R) of approximately 0.88. Finally, the ratio of Tb18-7H (horizontally polarized Tb at 18.7 GHz) to Tb36-5V was considered primarily as the quasi-emissivity, which is more reasonable and explicit in measuring the microwave radiation changes in soil freezing and thawing than the spectral gradient. By combining Tb36-5V to indicate the soil temperature variety, a Fisher linear discrimination analysis was used to establish the discriminant functions. After being corrected by TMMR measurements, the new discriminant algorithm had an overall accuracy of 86% when validated by 4-cm soil temperature. The multi-year discriminant results also provided a good agreement with the classification map of frozen ground in China. Copyright © 2011 John Wiley & Sons, Ltd.

KEY WORDS soil freeze/thaw status; microwave radiometer; discrimination analysis; AMSR-E

Received 24 February 2010; Accepted 11 October 2010

INTRODUCTION

Permafrost regions occupy approximately 22.79×10^6 km² or 23.9% of the exposed land area of the northern hemisphere (Zhang *et al.*, 1999, 2003b; Schwank *et al.*, 2004), while long-term average area extent of seasonally frozen ground occupy about 56% of the land surface, up to 80% in extreme years in the northern hemisphere (Zhang *et al.*, 2003b). Permafrost is also widespread in China with about 1.72×10^6 km² (Li *et al.*, 2008), and seasonal frozen soil accounted for more than half (Zhou *et al.*, 2000). In the permafrost zone, freezing and thawing processes have strong implications on hydrology and terrestrial ecology and in turn have a significant impact on the surface moisture and energy balance, hence on weather and climatology. For instance, increased frozen soil will reduce the hydraulic conductivity and impede water infiltration, which may promote water pooling on fields, surface runoff and soil erosion. Also, land surface heat exchange is strongly influenced by the presence of frozen soil and thus needs to be

considered in meteorological models (Kerr *et al.*, 2001). Freeze–thaw cycles as a strong indication of climate change have been paid much more attention in recent studies.

The study of freezing and thawing processes of the surface soil has been mainly based on site-measured data (Zhou *et al.*, 2000). This traditional method is time consuming and less representative of the whole region. However, it is quite necessary for real-time monitoring the spatial and temporal extent of frozen soil or even its characteristics distribution, such as frozen depth and phase transition water content during freeze–thaw processes. Satellite remote sensing technology, in particular microwave remote sensing, has a full-time and all-weather capability to monitor the large-scale freeze–thaw status and its changes and is a highly efficient means to do so. Recently, its monitoring has been considered as a key component of the National Aeronautics and Space Administration (NASA) Soil Moisture Active and Passive (SMAP) mission (Entekhabi *et al.*, 2004, 2010). The mission data will enable advances in climate prediction and global change studies.

Researchers have conducted a number of experimental studies and theoretical calculations on the use of passive

*Correspondence to: Lixin Zhang, School of Geography and Remote Sensing Science, Beijing Normal University, Beijing 100875, China.
E-mail: lxzhang@bnu.edu.cn

microwave data to detect the freeze/thaw status of ground surfaces. Wegmüller (1990) carried out measurements on frozen and unfrozen soil using a ground-based radiometer and scatterometer system between 3 and 11 GHz. It was found that an additional wet layer was formed at the soil surface during the thawing process, which could cause a strong influence on the microwave radiation. The Scanning Multi-channel Microwave Radiometer (6.6, 10.7, 18, 21 and 37 GHz) was initially used for freeze/thaw classification by Zuerndorfer *et al.* (1990a,b). It was found that the 18–37 GHz spectral gradient (SG) was a good indicator of the frozen and thawed ground, and Tb37 with high correlation to soil temperature was used as an additional criterion for discrimination. England *et al.* (1991) gave an explanation that negative SGs are caused by volume scatter darkening within the frozen soil. The argument is that freezing reduces the imaginary part of the moist soil dielectric constant, proportionally more than it does for the index of refraction. The effective emitting depth is increased so that frozen soils are more transparent to microwaves than are moist soils. In 1992, Zuerndorfer and England showed that a low value of Tb37 and a negative SG are effective discriminants for classifying soils as frozen. On the basis of passive microwave signatures from 5 to 100 GHz, Mätzler (1994) also found that large differences exist between frozen and unfrozen bare soil. In 1997, Judge *et al.* believed that the Zuerndorfer's algorithm should be adjusted when using the SSM/I (Special Sensor Microwave Imager) data, which have 19.35, 22.235, 37 and 85.5 GHz radiometers with dual polarizations at all frequencies except the 22.235 GHz water vapour channel. Similarly, Tb37 and the 19–37 GHz SG with vertical polarization were selected to classify frozen and thawed soils. Zhang and Armstrong (2001) and Zhang *et al.* (2003a) obtained a cut-off brightness temperature (Tb) of 258.2 K based on a linear correlation between the soil temperature at 5 cm depth and the Tb37V, so that the threshold in the Judge's method was modified. At the same time, they found that this algorithm could not detect the soil freeze/thaw status under snow cover. Recently, using SSM/I data, Jin *et al.* (2009) developed a decision tree algorithm including scattering index, Tb37V and 19 GHz polarization difference, and took into account the scattering effect of desert and precipitation.

From the above reviews, several issues are still uncertain and need further study. (1) It seems to lack adequate theoretical and experimental support that the frozen soils have a negative SG (England *et al.*, 1991). It does not always appear through substantial measurements (Zhang *et al.*, 2009). The arisen volume scattering effects and decreased permittivity may be inadequate to induce an inversion of high and low frequency Tb. (2) The effects of vegetation and snow on the discrimination algorithm have not been particularly evaluated in prior work. When applied to the regional monitoring, the original threshold and even algorithm need certain amendments because of the complex and volatile surface environments. (3) As the Earth Observing System Aqua satellite has been launched

for several years, its Advanced Microwave Scanning Radiometer Enhanced (AMSR-E) has 12 channels, collecting horizontally and vertically polarized data at frequencies of 6.9, 10.7, 18.7, 23.8, 36.5 and 89 GHz. It is more efficient in monitoring freeze–thaw cycles. However, there has been no intensive study on this new sensor. In view of the above questions, the development of a new discriminant algorithm under complex surface conditions is particularly necessary and important.

This study contributed to a new freeze/thaw discriminant algorithm with the new characteristics of AMSR-E data. Multi-channel microwave radiometer data of typical (wet and dry conditions) freezing and thawing processes in Biandukou and A'rou of the upper stream of Heihe River were collected. This was the first time changes in multi-channel microwave radiation of freezing and thawing soils under both wet and dry conditions were observed. A combined model was established to consider the effects of complex environmental conditions, which were often neglected in previous works. An innovative criterion was put forward to describe the difference of radiation between the frozen and thawed soil. It had a more explicit physical meaning and was believed more appropriate than the SG. By combining the simulated and observed data, the objective of this article was to develop an accurate and reliable method of detecting the freeze/thaw status of soils from AMSR-E data and to meet the demand for long sequence frozen soil data sets. At last, the discriminant results were validated by a regional data set over Tibet and compared with a classification map in China. Figure 1 is a flowchart representing the procedure of this study.

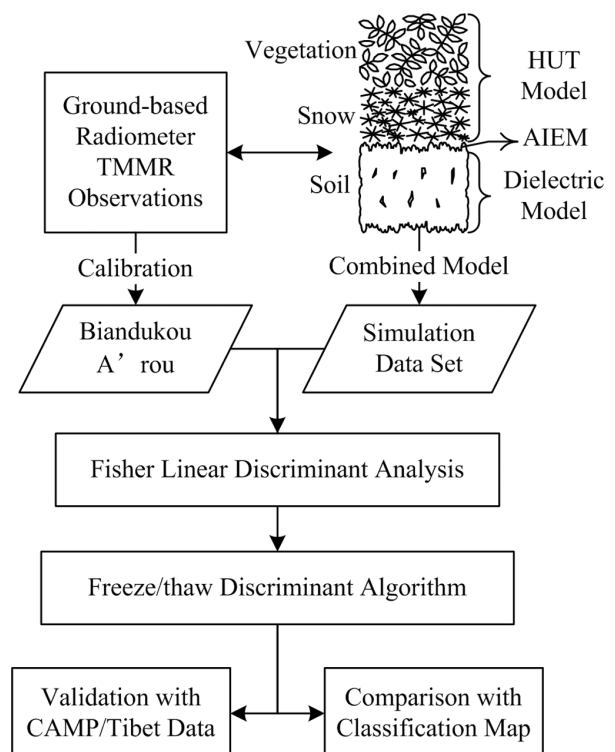


Figure 1. Flowchart of the research procedure

The Section on Experimental Data contained a detailed description of the experimental data and the changes in radiation characteristics of the freeze–thaw process. In the Section on Radiation Simulation, a combined model was established for complex ground environments, and simulation results were discussed. The Section on Discrimination Algorithm provided the establishment and correction of the discriminant algorithm, and the validation was carried out in Section on Comparison Validation. The conclusions were summed up in the last Section on Summary.

EXPERIMENTAL DATA

With the support of the Chinese Academy of Science, the Ministry of Science and Technology and local governments, the Watershed Allied Telemetry Experimental Research (WATER) was deployed from 7 March to 12 April 2008 in the Heihe River Basin, the second largest inland river basin in the arid regions of northwestern China (Li *et al.*, 2009). This is a simultaneous satellite-borne, air-borne and ground-based remote sensing and surface measurement experiment. A lot of remote sensing data and true ground data were collected.

Microwave radiometer system

Continuous observations of the freeze–thaw cycles on typical ground surfaces were conducted at 18.7 and 36.5 GHz with the Truck-mounted Multi-frequency Microwave Radiometer (TMMR) (Figure 2), which has four different frequency modules with dual polarizations of 6.925, 10.65, 18.7 and 36.5 GHz to be consistent with AMSR-E. Antennas at 6.925 and 10.65 GHz were under repair during the experiments.

This multi-frequency system was designed for field experiments by Radiometer Physics GmbH and Beijing Normal University. It consists of four components: antennas, a positioner, host software and the platform. At 6.925 and 10.65 GHz, two parabola plates were designed to generate beams with the desired half power beam width. The microwave emission of the scene collected by the antenna is first split into vertical and horizontal polarization components using an orthomode transducer. Then



Figure 2. Microwave radiometer system

the signal is amplified by a 40-dB low noise amplifiers (LNA) and filtered by waveguide band-pass filter before it is amplified by another 20-dB LNA. Finally, the measured information is processed and stored in a computer. The antenna performances in detail are listed in Table I.

A four-point calibration procedure was carried out for the instruments' absolute calibration before the experiments (Zhao *et al.*, 2008b). In each receiver, an internal ambient temperature calibration target was isolated by low- and high-density Styrofoam with no exchange of air between the interior and environment, and a thermal sensor was placed to measure its precise physical temperature. A liquid nitrogen (LN) cooled black body target was used as the cold calibration standard. The boiling temperature of the LN and the physical temperature of the cold load were calculated by the software (embedded with computer), taking into account the barometric sensor measured. There was also a stable noise diode in each receiver, which was used to correct detector diode non-linearity. By selecting or not selecting this noise source, another two-point calibration could be gained. Therefore, four formulae could be used to solve for the gain and the system noise of each receiver as well as the system nonlinearity and the noise temperature of the noise diode. The calibration error caused by microwave reflection at the LN/air interface was also automatically corrected by the calibration software. An absolute T_b accuracy of 1 K could be achieved with the accuracy of calibration target temperature sensors and the minimization of thermal gradients.

Ground-based measurements

As described in the Section on Introduction, information on the freeze–thaw cycle of the soils can be inferred from microwave radiometer data. Here, the results of radiometer observations were presented for two typical ground environments in the upper stream of Heihe River.

Biandukou. On 14 March, the radiometer was used to continuously measure a typical ground object of wheat stubble field in Biandukou (38°15'N, 100°55'E). The radiometer was set to work at incident angle of 20–70° in steps of 5°. The soil moisture at 0–1, 1–3 and 3–5 cm below the surface was measured by the traditional weighting method. As there was not significant change in soil moisture during the observation, the mean value of 0–1 cm was used as the effective value for the ground surface. A platinum-resistance thermometer was used to measure the soil temperature at 0–1 cm every half-hour, and the roughness of the ground was confirmed

Table I. Performance of corrugated feed/parabola antenna

Frequency (GHz)	6.925	10.65	18.7	36.5
Side-lobe level (dB)	<–30	<–35	<–40	<–40
Directivity (dB)	28.3	29.6	25.6	25.6
HPBW (°)	6.85	6.11	10.25	10.25

Table II. Ground parameters around the radiometer in Biandukou and A'rou

	Sand content (%)	Clay content (%)	Bulk density (g/cm ³)	Gravimetric soil moisture (%)	RMS height (cm)
Biandukou	13.82	11.03	1.06	5.1	2.8
A'rou	28.66	10.3	0.83	26.4	2.5

by grid plate and digital camera. All parameters measured are listed in Table II.

The whole process from thawed to frozen was observed from 11:00 to 24:00 hours, but about 100 min (from 16:50 to 18:30 hours) radiometer data were lost due to generator problems. The data loss did not preclude our analysis. The Tb at an incident angle of 55° was selected to be consistent with AMSR-E, and the values (four values obtained per minute) were averaged to one value for every minute. The physical temperature in every minute was obtained by the regression based on the half-hour observation. Then, the Tb was divided by the physical temperature to calculate the emissivity of ground. The SG was calculated using formula (1), in which the subscript p presents the polarization mode. The continuous observation results are shown in Figure 3.

$$SG = \frac{(Tb_{36.5,p} - Tb_{18.7,p})}{(36.5 - 18.7)} \quad (1)$$

During the day, it was quite evident that the Tb changes with ground temperature. The Tb curves had some fluctuation, but the physical temperature did not due to discontinuous measurements. After 18:54 hours, the temperature dropped below the freezing point, but the Tb remained nearly unchanged as the temperature dropped. This was because the unfrozen water content decreased when the temperature was dropping, and this caused a rise in emissivity which can prevent the Tb

from dropping. At the same time, it can be seen that the emissivity of the ground obviously rose when the soil became frozen. However, the increase in emissivity caused by freezing was small because the surface soil was dry with a gravimetric water content of 5.1%.

Also, it can be seen that the difference between Tb18.7 and Tb36.5 became smaller over time for both polarizations. This was embodied more clearly in the change of emissivity and SG. A negative SG was not observed in this experiment, but the SG became smaller when the ground became frozen. The SG in horizontal polarization dropped to 0.247 K/GHz for frozen soil from 0.346 K/GHz for thawed soil, and the SG in vertical polarization dropped to 0.066 from 0.184 K/GHz. This was caused by both changes in unfrozen water content and volume scattering. Tb18.7 was more sensitive to soil moisture content, thereby having a larger increase in emissivity than Tb36.5. Moreover, volume scattering at a high frequency was greater than at low frequency. There was a greater hindrance with Tb36.5 with increasing emissivity than with Tb18.7. These two effects were consistent with the lowering of the SG of frozen soil.

During the whole process, the Tb36.5 was higher than Tb18.7 in each polarization. It was worth noting that the emissivity at 36.5V was the most stable in the whole freeze–thaw process due to its small dependency of the dielectric property of surface soil on the water content. It produced a high sensitivity of Tb36.5V on physical temperature. On the other hand, the emissivity at 18.7 H had largest changes.

A'rou. On 10 and 11 March, a piece of grassland with snow covering in A'rou (38°02'N, 100°26'E) was selected for observation. The snow-free land was prepared by removing a thin snow layer, but there were still a few ice particles left. According to the vision field range of the radiometer, snow-free land was observed at 240° of azimuth with incident angle at 50°. Also, four temperature probes with thermal resistor were buried in the soil. The probes were connected with a data logger (Datataker, DT85) to automatically measure temperatures of near-surface air and at 0–1, 1–4 and 4–7 cm below the surface soil every minute. Two pieces of snow-free land were selected for measuring soil moisture at 0–2 cm and other parameters of soil. The statistical results are given in Table II.

The observation process from frozen to thawed state began at 21:00 hours on 10 March and finished at 13:30 hours the next day. About 20 values can be measured every minute by the radiometer on the snow-free land. As there was only one physical temperature value every minute, the Tb measurements were averaged

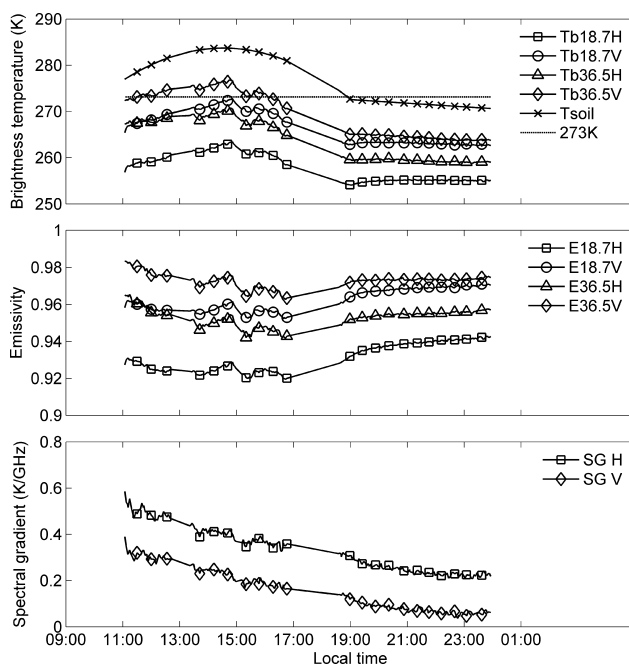


Figure 3. Observed Tb, calculated emissivity and spectral gradient of a wheat stubble field in Biandukou

to one value for 1 min. Temperature at 0–1 cm below the surface was considered to be the physical temperature for snow-free land. Observed Tb, calculated emissivity and SG are shown in Figure 4.

This observation site was quite different from the one in Biandukou. The Tb did not follow the physical temperature and then went down when the soil thawed at about 10:10 hours. This was because the initial gravimetric soil moisture was as high as 26.4%, and more water phase transition occurred altering the dielectric properties to decrease the emissivity of soil. In the thawing process, the real part of dielectric constant of soil was going up and the volume scattering was decreasing with the increasing liquid water in the soil, which made the microwave radiation from soil become smaller. When the ground surface was completely frozen, the emissivity appeared quite stable, whereas Tb varied with physical temperature.

The SG in horizontal polarization was 0.123 K/GHz for frozen soil compared with 0.892 K/GHz for thawed soil, and the SG in vertical polarization increased from –0.029 K/GHz for frozen soil to 0.276 K/GHz for thawed soil. There was a more evident change of SG than with dry soil, especially in horizontal polarization. Accordingly, the SG is more effective in judging the freeze–thaw status when the soil is wet enough. Due to the small sensitivity of dielectric property to moisture content, there was a minimal change in Tb36.5V.

To sum up, the microwave emissivity of soil will increase and the SG will decrease as the soil becomes frozen. The cause is the changes in dielectric properties and volume scattering. This phenomenon is more pronounced when the soil is wet. In addition, soil textures (sand and clay content) also have an influence on Tb behaviour, because the differences in soil particle size

distribution would affect the soil binding force on water, and then affect the freezing speed and level of soil.

RADIATION SIMULATION

Typical experimental results are shown and discussed in the Section on Ground-based Measurements. But only two sites' data are not enough to develop an algorithm. Diverse ground environments of the freeze/thaw soils need to be considered with a simulation model. In this section, simulation models were developed which can predict the observed experimental results correctly. The first part below introduced a combined model consisting of three modules. The second part showed the results of the simulation.

Simulation models

Microwave radiation from the ground is affected by various factors such as vegetation and snow. In order to get rid of these interferences, a discrimination algorithm should take into account the effects from complex ground environments, and the simulation model for algorithm developing should be able to calculate these effects. In this study, a combined microwave emission model was established for simulation. A dielectric constant model for frozen soil was used to calculate the dielectric properties of freeze–thaw soil, and the advanced integral equation method (AIEM) was introduced to describe the surface scattering. On this basis, the Helsinki University of Technology (HUT) snow microwave emission model considered the effects of snow and vegetation.

Dielectric constant model for frozen soil. At microwave bands, electromagnetic emissivity from the surface with a certain roughness is mainly determined by the dielectric constant of soil. This is a function of many parameters including soil moisture, temperature and frequency. In particular, the moisture content has a decisive impact on the dielectric properties of soil. Based on previous studies, Dobson *et al.* (1985) developed a semi-empirical model to calculate the dielectric constant of soil, and it has been widely used in the field of microwave remote sensing. The expression is

$$\varepsilon_m^\alpha = 1 + (\rho_b/\rho_s)(\varepsilon_s^\alpha - 1) + m_v^\beta \varepsilon_{fw}^\alpha - m_v \quad (2)$$

where ρ_b and ρ_s are bulk density and specific density of soil, respectively, m_v presents volumetric soil moisture, α is a constant shape factor and β is a soil texture-dependent coefficient. The subscripts s and fw refer to solid soil and free water, respectively.

However, not all liquid water freezes below the freezing point. Based on the semi-empirical dielectric mixing model for soil–water mixture, Zhang *et al.* (2003c) used an empirical function to estimate the fractions of liquid water and ice in frozen soil, and added a new term to the Dobson's model to consider the contribution of the ice fraction. The estimated results were well validated with

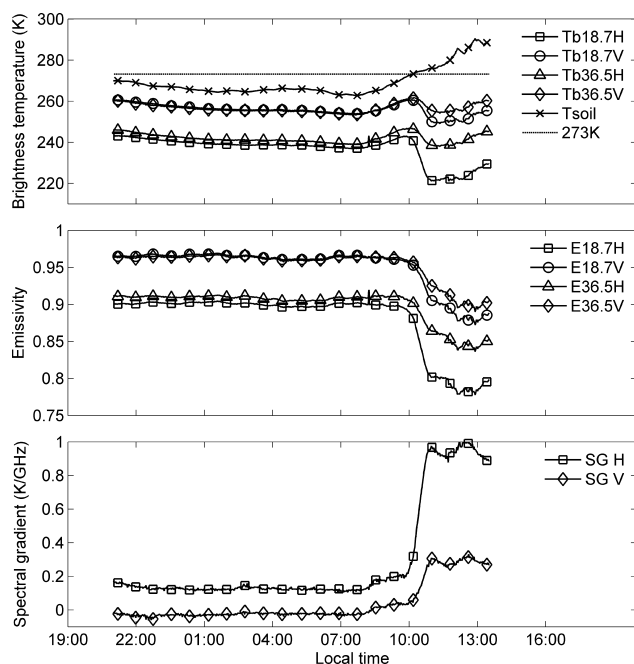


Figure 4. Observed Tb, calculated emissivity and spectral gradient of snow-free grassland in A'rou

dielectric measurements by an Agilent PNA Network Analyzer. The expression for calculating the dielectric constant of the soil–water–ice mixture can be written as

$$\varepsilon_{mf}^{\alpha} = 1 + (\rho_b/\rho_s)(\varepsilon_s^{\alpha} - 1) + m_{vu}^{\beta}\varepsilon_{fw}^{\alpha} - m_{vu} + m_{vi}\varepsilon_i^{\alpha} - m_{vi} \quad (3)$$

where vu refers to unfrozen water content, vi is the volumetric ice content, $\alpha = 0.65$, and the expressions for calculating β are adapted to Equation (3). The amount of unfrozen water is mainly dependent on soil temperature and the characteristics of soil. The relationship is expressed as (Zhang *et al.*, 2003c)

$$m_{vu} = a|T_{soil} - 273.15|^{-b}\rho_b \quad (4)$$

where T_{soil} is soil temperature in Kelvin, and a and b are constants determined by soil textures.

The dielectric constants of frozen and thawed soil would be estimated by Zhang's model, and the results are used in this article to analyse the characteristics of emission from soil during freezing and thawing.

AIEM surface scattering model. At the interface between two homogeneous media, the scattering characteristics are determined by the interface roughness and the dielectric discontinuity between the media. The surface roughness can be described with two parameters of root mean square (RMS) height and correlation length. The RMS height characterizes the surface roughness along the vertical direction, and the correlation length describes the horizontal characteristics of the surface. Researchers have developed several surface scattering models such as the small perturbation model, Kirchhoff model, phase perturbation model and the full wave model (Fung, 1994). These models are all limited and have their own fields of application.

Fung *et al.* (1992) put forward an integral equation method (IEM), a surface scattering model based on the electromagnetic radiation transfer equation. The model was verified by laboratory measurements of bistatic scattering from surfaces with small-, intermediate- and large-scale roughness and has been widely used in simulation and analysis of microwave radiation and scattering.

Chen *et al.* (2003) improved the IEM model by retaining the absolute phase term in the Green's function, which made this advanced IEM (AIEM) more accurate than IEM. The AIEM simulation results at L-band with small RMS height and correlation lengths agreed with the simulations using three-dimensional method of moment Monte Carlo (Chen *et al.*, 2003). Shi *et al.* (2005) compared the AIEM results with ground experimental data at AMSR-E frequencies over a wider range of roughness and dielectric constants. The results showed that the predicted surface emissivity is very similar to that of the experimental data. Zhanget *al.* (2004) used AIEM to simulate the emission characteristics of frozen soil surface at C, X and Ku bands and achieved the desired results. By

assuming the freeze/thaw soil performs as a homogeneous semi-infinite space, this article applied AIEM to deal with the soil boundary effects, and the volume scattering was ignored because of the small penetration depth and the dominant surface scattering.

The T_b of bare soil can be expressed as

$$T_{B,soil} = (1 - R_0)T_{soil} \quad (5)$$

where R_0 is the reflectivity at the soil–air boundary.

HUT snow emission model. In the HUT snow microwave emission model (Pulliainen *et al.*, 1999), the radiative transfer-based semi-empirical model describes the emission behaviour of a homogeneous snowpack as a function of water equivalent, effective grain size and density of the snow. In addition, the modelling approach takes into account the influence of the soil surface, forest canopy and atmosphere to space-borne observed T_b by using empirical and semi-empirical formulas.

For a homogeneous snow layer with a certain thickness, the underlying soil is treated as frozen soil. The following formula for the emitted T_b just below the snow–air boundary is used

$$T_{B,snow} = (1 - R_2) \left[(1 - R_1)T_{soil}e^{-(k_e - qk_s) \sec \theta d} + \frac{k_{\alpha}T_{snow}}{k_e - qk_s}(1 - e^{-(k_e - qk_s) \sec \theta d}) \right] \quad (6)$$

where k_{α} is an absorption coefficient, k_s is a scattering coefficient, k_e is an extinction coefficient and q is a purely empirical constant, evaluated to be 0.96 for all frequencies. R_1 and R_2 are the reflectivity at the soil–snow and snow–air boundary, which are calculated by AIEM and Fresnel reflection equations (Fung, 1994), respectively. T_{soil} and T_{snow} are effective temperatures for soil and snow layer. The first term corresponds to the T_b contribution originating below the snow layer and attenuated by the snow layer. The second term is the actual microwave emission contribution of the homogeneous snow layer.

The T_b of a forested terrain is modelled ignoring the scattering by forest canopy. The physical temperatures of soil, snow and canopy are assumed to be equal for simplicity (Pulliainen *et al.*, 1999; Zhao *et al.*, 2008a)

$$T_{B,can} = [1 - (1/L_{can}^2)(1 - e_{soil})]T_{phys} \quad (7)$$

$$T_{B,snow,can} = [1 - (1/L_{can}^2)(1 - e_{snow})]T_{phys} \quad (8)$$

where L_{can} is forest canopy loss factor that is correlated to frequency and forest stem volume.

In Pulliainen's work (1999), the comparison of model predictions with independent experimental data shows good correlations, especially in terms of the spectral characteristics. Recently, some experimental validation activities were also conducted against tower-based and air-borne radiometer data by Lemmetyinen *et al.* (2009). However, this model describes the snowpack as a single layer with average snow parameter inputs. It is limited

when applied to a vertically strongly stratified snowpack, comparing with the microwave emission model of layered snowpacks (Wiesmann and Mätzler, 1999) and the new multi-layer version of HUT snow emission model (Lemmetyinen *et al.*, 2010). But as the former single-layer version is relatively simple, it was used here to consider the impacts of snow and vegetation in our freeze–thaw study.

Combined model for cold land. As various land covers may disturb the discrimination of freeze–thaw soil, a general model that is available for simulating microwave radiation from freeze/thaw soil under complex ground environments is required. For this purpose, a combined model for cold land was set up and consists of three main modules: freeze/thaw soil dielectric constant estimation, calculation of emission from bare soil and Tb of the complex ground with snow or forest canopy.

First of all, the dielectric constant model was used to estimate the permittivity of freeze/thaw soil, in succession, which was used as the inputs to AIEM to deal with the randomly rough soil–air or soil–snow interface. Then, the Tb of snow-covered ground can be calculated using Equation (6). The Tb of canopy-covered ground can be determined using Equation (7). Similarly, the model calculated the Tb of ground with both snow and canopy covered using Equation (8).

When it comes to the mixed pixel, a large variety of pixel pattern may be present. The overall Tb of the whole scene is assumed to be a linear combination of each cover fraction as

$$T_B = f_{\text{soil}}T_{B,\text{soil}} + f_{\text{snow}}T_{B,\text{snow}} + f_{\text{can}}T_{B,\text{can}} + (1 - f_{\text{soil}} - f_{\text{snow}} - f_{\text{can}})T_{B,\text{snow,can}} \quad (9)$$

where f_{soil} , f_{snow} and f_{can} are the fraction of soil, snow and forest canopy in the mixed pixel, respectively.

With this combined model for cold land, it is possible to simulate and analyse the microwave emission characteristics of freeze/thaw soil with diverse ground environments. It is the main foundation for the establishment of the discrimination method of the freeze/thaw state in the rest of the article.

Simulation results

As the wheat stubble and grass in Biandukou and A'rou are both dry, the impacts on microwave signals can be neglected (Zheng *et al.*, 2009). They were treated as bare soil, and the supporting measured ground parameters

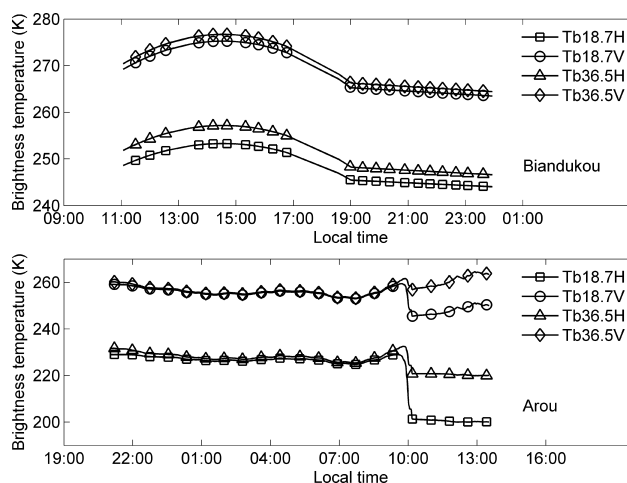


Figure 5. Simulated Tb in Biandukou and A'rou

were imported into the combined model for simulation. The results are shown in Figure 5.

The simulation and measured results both indicated that microwave radiation of freezing soil would decrease in dry conditions (Biandukou), but increase in wet conditions (A'rou). These changes were predicted correctly by the combined model. To further analyse the applicability of the combined model, we calculated root mean square errors (RMSE) and relation coefficients (R) of the model simulations as compared with the observations in Table III. The model simulations quite followed the trend of *in situ* observations with an overall R of approximately 0.88. It had a good agreement at vertical polarization with a RMSE of 2.16 K. However, the model overestimated the polarization difference, due to the Tb at horizontal polarization being underestimated with a RMSE of 12.95 K. There were also some details that have not been caught by the model, because many other uncertain factors were not accounted for.

In general, the model simulations and field observations are consistent. Results indicate a model response to the change of soil freeze–thaw status. The underestimation bias at horizontal polarization is acceptable as it can be corrected through the measured data during algorithm development. The simulation accuracy of HUT model over snow and forest is not carried out here again, because it has been well validated as discussed above and its performance was analysed and validated preliminarily by Zhao *et al.* (2009). The observations and simulations presented here both indicated that each channel reflects information of different aspects in the freeze–thaw process, and the multi-channel data are critical in improving the accuracy in the freeze–thaw status determination.

Table III. RMSE and R of model simulations as compared with field observations

		18.7 H	18.7 V	36.5 H	36.5 V	Mean H	Mean V
RMSE (K)	Biandukou	9.3263	3.0631	12.4491	1.3750	12.9465	2.1623
	A'rou	15.0936	2.1673	14.9171	2.0436	—	—
R	Biandukou	0.9751	0.9877	0.9557	0.9706	0.8849	0.8749
	A'rou	0.9442	0.8524	0.6646	0.6888	—	—

DISCRIMINANT ALGORITHM

This section examined the establishment of a classification algorithm. The first part provided the physical mechanism and effects of the criteria. In the second part, several discriminant functions were established using simulation data sets, and the algorithm was calibrated at 18.7 GHz by radiometer measurements.

Criteria selection

Frozen ground is soil or rock in which part or all of the pore water has turned into ice (Everdingen, 2005). It indicates that there are mainly two characteristics to determine the ground to be frozen: low physical temperature and possible ice content. At microwave bands, there is a better correlation between Tb37V and surface temperature than other low-frequency data. McFarland *et al.* (1990) carried out extensive research on surface temperature inversion using microwave data and found that Tb37V is most suitable in estimating surface temperature. The inaccuracy of the algorithm using 37 V as the main channel is $<1^{\circ}\text{C}$. On the other hand, the phase transition from water to ice can result in a large increase in emissivity, which is more obvious in the horizontal polarization at low frequencies. Thus, the ratio of Tb in the horizontal polarization at low frequency (6.925, 10.65 and 18.7 H) to 36.5 V can be used to indicate the variation of emissivity. This ratio will be called as the quasi-emissivity in the following text. Consequently, the quasi-emissivity and quasi-temperature (Tb36.5V) are two selected criteria for freeze–thaw soil classification in this article.

Microwave radiation from the ground is influenced by many various factors, such as temperature, soil moisture, surface roughness, soil texture and other snow or vegetation parameters, which may have an important effect on determining the freeze–thaw status of soil. Thus, the classification algorithm should be established considering these interference factors. However, the ordinary experimental data cannot meet this demand because of its limitations on covering diverse environmental conditions. With that in mind, the combined model for cold land above was used to simulate the emission from six typical ground environments: frozen bare soil, thawed bare soil, frozen soil with forest, thawed soil with forest, frozen soil with snow and frozen soil with snow and forest. These ground surfaces were treated as pure pixel. For each typical ground type, 100 groups of multi-channel Tb data were simulated with random parameter inputs. The input parameters are random values with corresponding reasonable ranges or static constants (Table IV) that

cover the general changes in the surface parameters. The soil temperatures between -1 and 1°C were avoided to guarantee the soils were exactly frozen or thawed. The incident angle was 55° in correspondence with AMSR-E.

Figure 6 showed the random simulation results displayed as Tb36.5V and the quasi-emissivity at 18.7 H. It can be seen that the freeze–thaw soil under different ground conditions is clearly separated by these two criteria. Taking the bare soil with a scattered distribution as an example, the quasi-emissivity and Tb of wet soil are very low, and it can be distinguished from frozen soil by the quasi-emissivity. Dry soil has a higher quasi-emissivity and Tb, but it can be distinguished from frozen soil by the quasi-temperature of Tb36.5V. When the frozen ground is covered by thin snow (snow depth <0.1 m), the volume scattering inside the snow layer makes the radiation characteristics similar to frozen bare soil, which has a lower quasi-temperature and a higher quasi-emissivity. When the snow is thick (snow depth >0.4 m) or the snow particles are large (diameter >1 mm), the volume scattering of the snow layer at 36.5 GHz is much higher than 18.7 GHz, and this causes Tb36.5V to decrease faster than Tb18.7H. It results in a significant increase in quasi-emissivity with values even more than 1. This also indicated that it is difficult to distinguish frozen soil from thin snow-covered ground. The data points with forest cover are more concentrated in Figure 6 due to microwave emission from vegetation and presents more easily to be distinguished than bare soil. On the whole, an important separability was generated by the two criteria

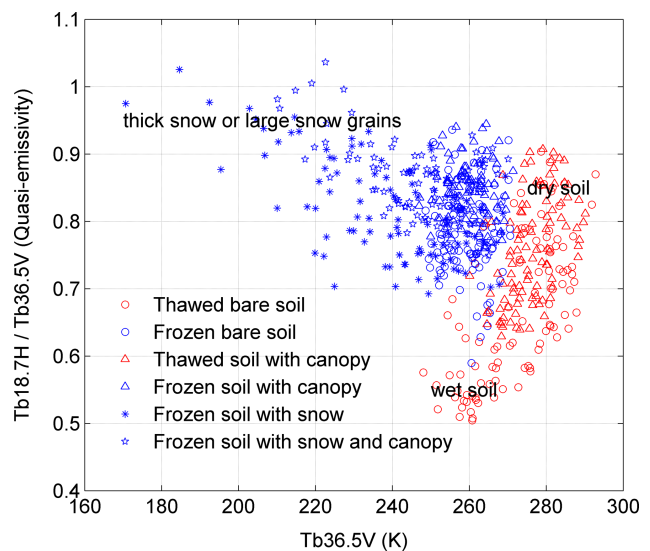


Figure 6. Random simulation results of microwave radiation from six typical ground surfaces

Table IV. Input parameters in the simulation with the combined model

Dielectric constant model	Sand content	10–30%	Clay content	20–40%
	Bulk density	0.5–1.5 g/cm ³	Specific density	2.6 g/cm ³
	Soil temperature	1–20°C, –20 to –1°C	Initial volumetric soil moisture	2–44%
AIEM model	RMS height	0.1–3 cm	Correlation length	10–40 cm
HUT model	Snow density	0.1–0.4 g/cm ³	Snow grain diameter	0.2–1.2 mm
	Snow depth	0.05–0.5 m	Forest stem volume	25 m ³ /ha

of quasi-temperature and quasi-emissivity. They will be used in our new algorithm.

Fisher linear discrimination analysis

The Fisher linear discrimination analysis (LDA) is a technique that well separates the observed data (Fisher, 1936). The main idea is to project data onto a line and perform classification in this one-dimensional subspace. The projection is found to maximize the distance between the means of the two classes while minimizing the variance within each class. Thus, the Fisher LDA is to project on line in the direction w which maximizes

$$J(w) = \frac{(\mu_1 - \mu_2)^2}{S_1^2 + S_2^2} \quad (10)$$

where μ represents a mean, S^2 represents a variance and the subscripts denote the two classes.

With projected data, an observation is classified into a certain group if the squared distance (also called the Mahalanobis distance) of the observation to the group centre (mean) is minimum. In this article, the training data set are input into SPSS application to construct the prediction model. The output from SPSS includes equations for each group from Fisher linear discriminant function. The general form of the equation is

$$D = m_1x_1 + m_2x_2 + n \quad (11)$$

where D is the discriminant score, m is the classification function coefficient, n is a constant value and x is the discriminant variable. For any observation, the group with the smallest squared distance has the largest discriminant score and the observation is then classified into this group.

The simulated quasi-emissivity at 6.925, 10.65 and 18.7 H and Tb36.5V that embody the change in the characteristics of freeze–thaw process best were selected as the training samples to establish the discrimination functions. The results of Fisher LDA are shown in Table V.

The discrimination results showed that the classification accuracy decreases with increasing frequency. It was indicated that the sensitivity of low frequency to soil moisture is more helpful in determining the freeze–thaw status than high frequency. However, the algorithm presented in this article was to use 18.7 and 36.5 GHz high-frequency data. This is because a global survey conducted by Njoku *et al.* (2005) reported that the radio

frequency interference (RFI) most likely happen at low frequency. Using high-frequency data could avoid the impact of RFI. On the other hand, the functions above were entirely based on simulation data that may cover diverse surface types and environmental conditions but are not entirely accurate. The ground measured data are more accurate, but cannot include many types of surface conditions, resulting in poor representation and a lack of data. It was believed that the combination use of simulated and observed data is able to avoid deviation in application. In order to ensure that the data are real and effective, all measured data points with physical temperature above 274.15 K were considered as thawed soil, and frozen soil below 272.15 K with the same number of thawed soils were selected. These screened true ground measurements (520 samples) by microwave radiometer were combined with the simulation data (600 samples) to determine the functions for correction. The corrected functions at 18.7 GHz are expressed as

$$D_F = 1.47 \text{ Tb}_{36.5} \text{ V} + 91.69 \text{ Qe}_{18.7} \text{ H} - 226.77 \quad (12)$$

$$D_T = 1.55 \text{ Tb}_{36.5} \text{ V} + 86.33 \text{ Qe}_{18.7} \text{ H} - 242.41 \quad (13)$$

where Qe refers to quasi-emissivity, and D_F and D_T are discriminant score for frozen and thawed soil, respectively. A class will be foretold to be frozen soil if D_F is greater than D_T . Otherwise, the class would be predicted as thawed soil.

COMPARISON VALIDATION

The new freeze/thaw discriminant algorithm presented in this article was developed with configurations of AMSR-E (Kawanishi *et al.*, 2003). This instrument measures radiation at six frequencies in the range 6.925–89 GHz with all dual polarization. The Aqua orbit is sun-synchronous with equator crossings at 13:30 and 01:30 hours local solar time, approximately corresponding to the hottest and coldest time of 1 day. This is advantageous when monitoring the freeze–thaw cycle. In order to evaluate the accuracy of the newly developed algorithm, the classification results were validated with a regional data set and a national map in this section.

The daily classification results were first compared with a regional data set obtained from the Coordinated Enhanced Observing Period (CEOP) Asia-Australia Monsoon Project (CAMP) over Tibet (Ma *et al.*, 2002). This data set contains observation stations over the central Plateau with the time period from 1 October 2002 through 31 March 2004. At each station, there may be different parameter measuring system for different science topics. The purpose of Soil Moisture and Temperature Measurement System (SMTMS) networks is to monitor soil moisture and temperature values and develop the land surface process models and satellite-based soil moisture retrieval methods. Before using the data of the SMTMS observations, a preliminary data quality assessment was performed. We selected four SMTMS stations

Table V. Coefficients of linear discriminant functions

		Constant	Tb36.5V	Quasi-emissivity	Accuracy (%)
6.925 H	F	−231.62	1.46	122.86	90.8
	T	−248.45	1.57	106.39	—
10.65 H	F	−235.36	1.45	131.41	90.5
	T	−252.15	1.56	114.81	—
18.7 H	F	−236.81	1.41	143.28	89.5
	T	−255.51	1.53	127.90	—

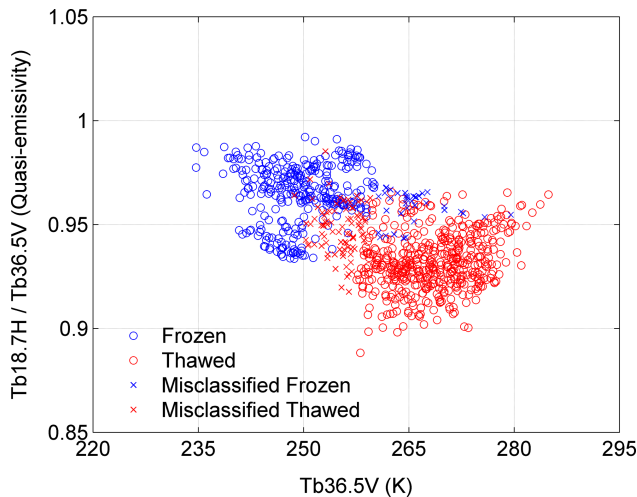


Figure 7. Comparison of discrimination results and 4-cm soil temperature observations at selected CAMP/Tibet stations

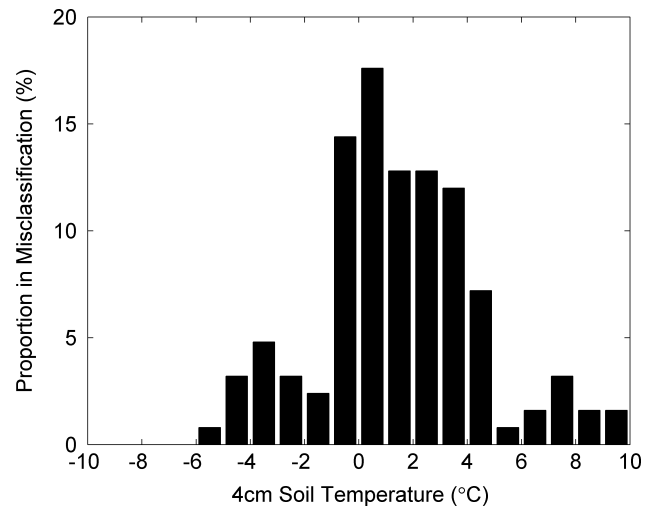


Figure 8. Frequency histogram of 4-cm soil temperature in misclassifications

(D66, D105, D110 and MS3608) with 4-cm soil temperature to carry out the validation. The multi-channel Tb over these stations was extracted from Aqua/AMSR-E L2A (V10) Global Swath products (Ashcroft *et al.*, 2006) at the local time of 13:30 hours for ascending. The soil temperature was recorded hourly, so the two records nearest to the satellite passing time were averaged as observed. Using the discriminant Equations (12) and (13), the pixels were well classified (Figure 7) with the two criteria of Tb36.5V and quasi-emissivity as expected. The number of validated pixels was 909, and 127 of them were misclassified. The overall classification accuracy was 86% (Table VI).

Frequency histogram of misclassified pixels is plotted against 4-cm soil temperature in Figure 8. It was found that most of the misclassifications occurred with the 4-cm soil temperature from -4 to 4°C . It indicated that most misclassifications occurred during the phase transition period between the warm and cold seasons. During this period, frequent phase transition happened at the soil surface, and there was always a phase difference between different depths of soil. The measured depth of soil temperature we were using was 4 cm, which was deeper than the penetration depth of 18.7 and 36.5 GHz microwave (Ulaby *et al.*, 1982). When the top layer soil (0–2 cm) had happened with the phase transition, the deeper soil at 4 cm had not occurred. This was considered to be the main reason of misclassifications in this validation case. Overall, the above long-term validation at regional scale showed that the discriminant

algorithm established in this article could classify the freeze/thaw status of ground soils correctly.

In order to further validate the reliability of the discriminant algorithm, we also conducted a comparison between multi-year classification results with the map of geocryological regions and classifications in China.

The AMSR-E data at level 3 (T05) were used (Njoku, 2008). It was assumed that there was no significant change of freeze/thaw status on two successive days, and Tb of these 2 days could be used to gain the full Tb map over the continent. For example, the no data area of ascending data on 1 January was filled up by the 2nd's, and the no data area of descending data on 2 January was filled up by the 1st's. Thus, the integral ascending and descending data sets of everyday were obtained. Then, the discriminant Equations (12) and (13) were used to determine the freeze–thaw status from 1 January 2004 to 31 December 2008. We supposed that it was a frozen day if freezing occurs during the day (ascending) or night (descending). The annual average number of frozen days of these 5 years is shown in Figure 9. It should be noted that the freeze–thaw state may be misjudged along the coastal zone because the radiometer observation there is strongly affected by mixed pixel composed of continent and ocean.

Compared with the map of geocryological regions and classifications (Qiu *et al.*, 2002, Figure 10), the permafrost regions which include high-latitude and high-altitude permafrost were discriminated with frozen days >180 days. Especially over the Tibet Plateau, the number of frozen days gradually increased from 180 days in the southeast to more than 360 days in the northwest. The regions with the frozen days varying from 3 to 180 days basically belonged to seasonally or short-time frozen ground, and the remaining areas with frozen days <3 days were considered as non-frozen areas in China. The detecting results (contours) agreed well with the distribution of frozen ground in China. However, the remote sensing results had more details than the classification maps. This could provide important information

Table VI. Discrimination results validation by 4-cm soil temperature observations at selected CAMP/Tibet stations

Station	Validation	Misclassification	Accuracy (%)
D105	259	40	84.56
D110	136	13	90.44
D66	259	36	86.1
MS3608	255	38	85.1
Total	909	127	86.03

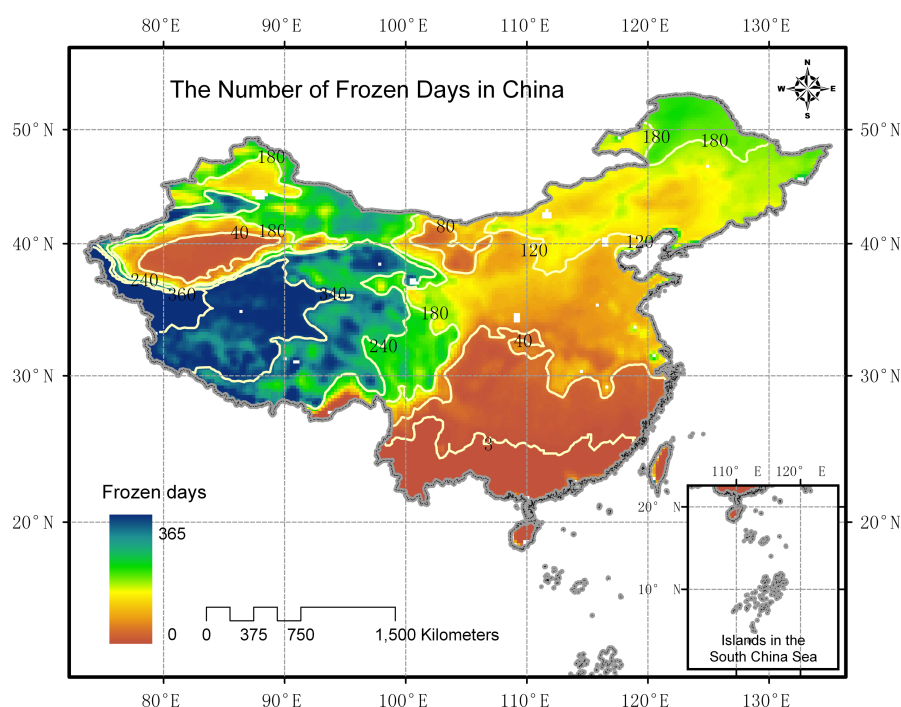


Figure 9. Detecting results of the annual average number of frozen days in China using AMSR-E

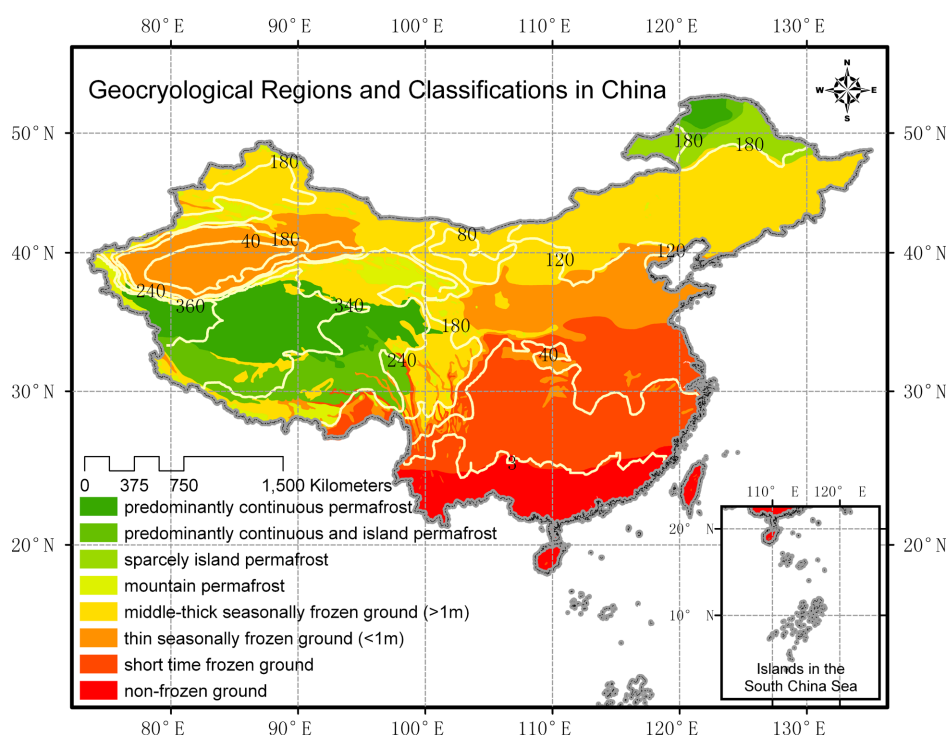


Figure 10. Map of geocryological regions and classifications in China

for geocryological classification revision in China and also reliable technical support for a real-time and wide range monitoring of permafrost.

SUMMARY

Seasonally frozen soils are widely distributed in the world and are sensitive to soil temperature as an indicator of climate change. Passive microwave remote sensing

has the advantages of high time resolution and wide spatial coverage, playing an important role in the study of the surface freezing and thawing process. In this article, with the new characteristics of AMSR-E, a new soil freeze/thaw discriminant algorithm was developed based on diverse simulation data and typical ground measurements by a TMMR. The average accuracy of the discriminant algorithm was 86% when validated with 4-cm soil temperature in CAMP/Tibet. The multi-year

averaged discriminant results were highly consistent with the map of geocryological regions and classifications in China. The main conclusions are summarized and discussed as below.

1. Measurements using a TMMR were carried out in the upper stream of Heihe River. It was the first time to show the time series of multi-channel microwave radiation of freezing and thawing soils under both wet and dry conditions. It was found that the microwave emissivity of soil increases and the SG decreases as the soil becomes frozen. The initial soil moisture content determines the direction and amplitude of radiation change in freezing soil. The microwave radiation of dry soil decreases when freezing, while the radiation of wet soil has a sharp increase. The main reasons are the changes in dielectric properties and volume scattering of freezing soil.
2. A combined model was established for cold land. With the outputs of a dielectric constant model of frozen soil, the AIEM model was used to deal with the rough boundary effects of freeze/thaw soil, and the HUT model was applied to consider the impacts of snow and vegetation, which have not been particularly evaluated in the previous work. The model simulations quite followed the trend of TMMR observations in Biandukou and A'rou with an overall R of approximately 0.88.
3. The ratio of Tb between 18.7° H and 36.5° V was considered originally as quasi-emissivity, which is a more reasonable and explicit way to measure the microwave radiation changes in soil freezing and thawing than a SG. Combining Tb36.5V to indicate the temperature variety, freeze/thaw soils under diverse conditions simulated randomly by the combined model was clearly separated by these two criteria. A Fisher LDA was used to establish the discriminate functions. After correction by the *in situ* measurements, this new discriminant algorithm had a high accuracy during verification.

This algorithm is limited over pixels which contain water body or lake ice, because these effects were not taken into account. This kind of error can be avoided by using a reliable water distribution map, and our criteria may not be valid for thawed soil with dry snow covered, which has a high quasi-emissivity and a low temperature. It could also have some problems with wet snow-covered ground, as passive microwave observations over melting snow cannot give information on the soil below. We are now conducting further experiments on the freezing and melting processes of snow to achieve possible progresses in this area. However, the validation results have showed that this new freeze/thaw discriminant algorithm based on AMSR-E can provide a long time series data set of reliable surface freeze/thaw state from the launch of AMSR-E in 2002 until now. The data set should be useful in the studies of permafrost science, frozen soil engineering, freeze–thaw erosion and global changing.

ACKNOWLEDGEMENTS

The study is jointly supported by Chinese State Key Basic Research Project (2007CB714403), National Natural Science Foundation of China (41030534), Public Sector (Meteorology) Special Research Project (GYHY200706044), CAS 10 Action Plan for West Development Program (KZCX2-XB2-09) and National High Technology Research and Development Program of China (2008AA12Z110). The authors are grateful for the CAMP/Tibet SMTMS data provided by CEOP project and AMSR-E Tb products provided by National Snow and Ice Data Center. The authors would also like to thank four anonymous reviewers, Xin Li of Cold and Arid Regions Environmental and Engineering Research Institute (CAS) and Jiancheng Shi of Institute for Computational Earth System Science (UCSB) for their valuable comments.

REFERENCES

- Ashcroft P, Wentz FJ. 2006. *AMSR-E/Aqua L2A Global Swath Spatially-resampled Brightness Temperatures V002*. National Snow and Ice Data Center. Digital media: Boulder, CO.
- Chen K, Wu T, Tsang L, Li Q, Shi J, Fung AK. 2003. Emission of rough surfaces calculated by the integral equation method with comparison to three-dimensional moment method simulations. *IEEE Transactions on Geoscience and Remote Sensing* **41**(1): 90–101. DOI: 10.1109/36.992784.
- Dobson MC, Ulaby FT, Hallikainen MT, El-Rayes MA. 1985. Microwave dielectric behavior of wet soil—Part II: dielectric mixing models. *IEEE Transactions on Geoscience and Remote Sensing* **GE-23**(1): 35–46. DOI: 10.1109/TGRS.1985.289498.
- England AW, Galantowicz JF, Zuerndorfer BW. 1991. A volume scattering explanation for the negative spectral gradient of frozen soil. *Proceedings of Geoscience and Remote Sensing Symposium* **3**: 1175–1177.
- Entekhabi DE, Njoku EG, Houser P, Spencer M, Doiron T, Kim Y, Smith J, Girard R, Belair S, Crow W, Jackson TJ, Kerr YH, Kimball JS, Koster R, McDonald KC, O'Neill PE, Pultz T, Running SW, Shi J, Wood E, Zyl JV. 2004. The hydrosphere state (Hydros) satellite mission: an earth system pathfinder for global mapping of soil moisture and land freeze/thaw. *IEEE Transactions on Geoscience and Remote Sensing* **42**(10): 2184–2195. DOI: 10.1109/TGRS.2004.834631.
- Entekhabi DE, Njoku EG, O'Neill PE, Kellogg KH, Crow W, Edelstein WN, Entin JK, Goodman SD, Jackson TJ, Johnson J, Kimball JS, Piepmeier JR, Koster R, Martin N, McDonald KC, Moghaddam M, Moran S, Reichle R, Shi JC, Spencer M, Thurman SW, Tsang L, Van Zyl J. 2010. The Soil Moisture Active Passive (SMAP) mission. *Proceedings of the IEEE* **98**(5): 704–716. DOI: 10.1109/JPROC.2010.2043918.
- Everdingen R. 2005. *Multi-language Glossary of Permafrost and Related Ground-Ice Terms*. National Snow and Ice Data Center/World Data Center for Glaciology: Boulder, CO.
- Fisher RA. 1936. The use of multiple measurements in taxonomic problems. *Annals of Eugenics* **7**: 179–188.
- Fung AK. 1994. *Microwave Scattering and Emission Models and Their Applications*. Artech House: Norwood, MA.
- Fung AK, Li Z, Chen K. 1992. Backscattering from a randomly rough dielectric surface. *IEEE Transactions on Geoscience and Remote Sensing* **30**(2): 195–200. DOI: 10.1109/36.134085.
- Jin R, Li X, Che T. 2009. A decision tree algorithm for surface soil freeze/thaw classification over China using SSM/I brightness temperature. *Remote Sensing of Environment* **113**: 2651–2660. DOI: 10.1016/j.rse.2009.08.003.
- Judge J, Galantowicz JF, England AW, Dahl P. 1997. Freeze/thaw classification for prairie soils using SSM/I radio brightnesses. *IEEE Transactions on Geoscience and Remote Sensing* **35**(4): 827–832. DOI: 10.1109/36.602525.
- Kawanishi T, Sezai T, Ito Y, Imaoka K, Takeshima T, Ishido Y, Shibata A, Miura M, Inahata H, Spencer RW. 2003. The Advanced Microwave Scanning Radiometer for the Earth Observing System (AMSR-E).

- NASDA's contribution to the EOS for global energy and water cycle studies. *IEEE Transactions on Geoscience and Remote Sensing* **41**: 184–194.
- Kerr YH, Waldteufel P, Wigneron J-P, Martinuzzi J, Font J, Berger M. 2001. Soil moisture retrieval from space: the Soil Moisture and Ocean Salinity (SMOS) mission. *IEEE Transactions on Geoscience and Remote Sensing* **39**(8): 1729–1735. DOI: 10.1109/36.942551.
- Lemmetyinen J, Kontu A, Qiu Y, Pulliainen J, Hallikainen M. 2009. Experimental validation activities of HUT snow emission model. *Proceedings of Geoscience and Remote Sensing Symposium* **2**: 871–874.
- Lemmetyinen J, Pulliainen J, Rees A, Kontu A, Qiu Y, Derksen C. 2010. Multi-layer adaptation of HUT snow emission model: comparison with experimental data. *IEEE Transactions on Geoscience and Remote Sensing* **48**(7): 2781–2794.
- Li X, Cheng GD, Jin HJ, Kang ES, Che T, Jin R, Wu LZ, Nan ZT, Wang J, Shen YP. 2008. Cryospheric change in China. *Global and Planetary Change* **62**(3–4): 210–218. DOI: 10.1016/j.gloplacha.2008.02.001.
- Li X, Li XW, Li ZY, Ma MG, Wang J, Xiao Q, Liu Q, Che T, Chen EX, Yan GJ, Hu ZY, Zhang LX, Chu RZ, Su PX, Liu QH, Liu SM, Wang JD, Niu Z, Chen Y, Jin R, Wang WZ, Ran YH, Xin XZ, Ren HZ. 2009. Watershed allied telemetry experimental research. *Journal of Geophysical Research* **114**: D22103. DOI: 10.1029/2008JD011590.
- Ma Y, Tsukamoto O, Ishikawa H, Su Z, Menenti M, Wang J, Wen J. 2002. Determination of regional land surface heat flux densities over heterogeneous landscape of HEIFE integrating satellite remote sensing with field observations. *Journal of the Meteorological Society of Japan* **80**(3): 485–501.
- McFarland MJ, Miller RL, Neale CMU. 1990. Land surface temperature derived from the SSM/I passive microwave brightness temperatures. *IEEE Transactions on Geoscience and Remote Sensing* **28**(5): 839–845. DOI: 10.1109/36.58971.
- Mätzler C. 1994. Passive microwave signatures of landscapes in winter. *Meteorology and Atmospheric Physics* **54**: 241–260. DOI: 10.1007/BF01030063.
- Njoku EG. 2008. *AMSRE-Aqua Daily L3 Surface Soil Moisture, Interpretive Parameters, & QC EASE-Grids*. National Snow and Ice Data Center. Digital media: Boulder, CO.
- Njoku EG, Ashcroft P, Chan TK, Li L. 2005. Global survey and statistics of radio-frequency interference in AMSR-E land observations. *IEEE Transactions on Geoscience and Remote Sensing* **43**(5): 938–947.
- Pulliainen JT, Grandell J, Hallikainen MT. 1999. HUT snow emission model and its applicability to snow water equivalent retrieval. *IEEE Transactions on Geoscience and Remote Sensing* **37**(3): 1378–1390.
- Qiu G, Zhou Y, Guo D, Wang Y. 2002. In *Maps of Geocryological Regions and Classifications*, Digitized by Zhang T (ed). National Snow and Ice Data Center/World Data Center for Glaciology. Digital media: Boulder, CO. In press.
- Schwank M, Stahli M, Wydler H, Leuenberger J, Mätzler C, Fluhler H. 2004. Microwave L-band emission of freezing soil. *IEEE Transactions on Geoscience and Remote Sensing* **42**(6): 1252–1261. DOI: 10.1109/TGRS.2004.825592.
- Shi J, Jiang L, Zhang L, Chen K, Wigneron J-P, Chanzy A. 2005. A parameterized multifrequency-polarization surface emission model. *IEEE Transactions on Geoscience and Remote Sensing* **43**(12): 2831–2840.
- Ulaby FT, Moore RK, Fung AK. 1982. *Microwave Remote Sensing: Active and Passive, Radar Remote Sensing and Surface Scattering and Emission Theory*, vol. II. Addison Wesley: Reading, MA.
- Wegmüller U. 1990. The effect of freezing and thawing on the microwave signatures of bare soil. *Remote Sensing of Environment* **33**(2): 123–135. DOI: 10.1016/0034-4257(90)90038-N.
- Wiesmann A, Mätzler C. 1999. Microwave emission model of layered snowpacks. *Remote Sensing of Environment* **70**: 307–316.
- Zhang T, Armstrong RL. 2001. Soil freeze/thaw cycles over snow-free land detected by passive microwave remote sensing. *Geophysical Research Letters* **28**(5): 763–766.
- Zhang T, Armstrong RL, Smith J. 2003a. Investigation of the near-surface soil freeze-thaw cycle in the contiguous United States: algorithm development and validation. *Journal of Geophysical Research* **108**(D22): 8860. DOI: 10.1029/2003JD003530.
- Zhang T, Barry RG, Knowles K, Ling F, Armstrong RL. 2003b. Distribution of seasonally and perennially frozen ground in the northern hemisphere. In *Proceedings of the 8th International Conference on Permafrost*, Zürich: Switzerland; vol. 2: 1289–1294.
- Zhang T, Barry RG, Knowles K, Heginbottom JA, Brown J. 1999. Statistics and characteristics of permafrost and ground-ice distribution in the northern hemisphere. *Polar Geography* **23**(2): 147–169. DOI: 10.1080/10889370802175895.
- Zhang L, Shi J, Zhang Z, Zhao K. 2003c. The estimation of dielectric constant of frozen soil-water mixture at microwave bands. *Proceedings of Geoscience and Remote Sensing Symposium* **4**: 2903–2905.
- Zhang L, Zhao S, Jiang L. 2009. The time series characteristic of microwave radiation of typical land surface in the Heihe upstream watershed during freeze/thaw season. *Journal of Glaciology and Geocryology* **31**(2): 198–206, (in Chinese).
- Zhang L, Zhao K, Zhu Y, Qin B. 2004. Simulated radiation characteristics of frozen soil surface at typical microwave bands. *Proceedings of Geoscience and Remote Sensing Symposium* **6**: 4310–4313.
- Zhao T, Jiang L, Zhang L, Du J. 2008a. Comparison of dry snow emission model and the primary study on satellite data simulation. *Proceedings of Geoscience and Remote Sensing Symposium* **4**: 1042–1045.
- Zhao S, Zhang L, Zhang Z. 2008b. Design and test of a new truck-mounted microwave radiometer for remote sensing research. *Proceedings of Geoscience and Remote Sensing Symposium* **2**: 1192–1195.
- Zhao T, Zhang L, Jiang L, Shi J, Zhao S, Pan J, Chai L, Zhang Y. 2009. A combined microwave emission model for cold land. *Proceedings of Geoscience and Remote Sensing Symposium* **2**: 314–317.
- Zheng Y, Zhang L, Xing W, Zhang Z. 2009. Study of the effects of vegetation on microwave radiation of frozen soil in cold regions. *Journal of Glaciology and Geocryology* **31**(2): 214–219, (in Chinese).
- Zhou Y, Guo D, Qiu G, Cheng G, Li S. 2000. *Geocryology in China*. Science Press: Beijing; 9, (in Chinese).
- Zuerndorfer B, England AW. 1992. Radiobrightness decision criteria for freeze/thaw boundaries. *IEEE Transactions on Geoscience and Remote Sensing* **30**(1): 89–102. DOI: 10.1109/36.124219.
- Zuerndorfer B, England AW, Dobson MC, Ulaby FT. 1990a. Mapping freeze/thaw boundaries with SMMR data. *Journal of Agriculture and Forest Meteorology* **52**(1–2): 199–225. DOI: 10.1016/0168-1923(90)90106-G.
- Zuerndorfer B, England AW, Ulaby FT. 1990b. An optimized approach to mapping freezing terrain with SMMR data. *Proceedings of Geoscience and Remote Sensing Symposium* **1**: 1153–1156.